VLA Observations of a New Population of Blazars

Hermine Landt
Harvard-Smithsonian Center for Astrophysics, 60 Garden Street, Cambridge, MA 02138.

Eric S. Perlman
Joint Center for Astrophysics, University of Maryland, 1000 Hilltop Circle, Baltimore, MD 21250.

Paolo Padovani
European Southern Observatory, Karl-Schwarzschild-Str. 2, D-85748 Garching, Germany.

ABSTRACT

We present the first deep VLA radio images of flat-spectrum radio quasars (FSRQ) with multiwavelength emission properties similar to those of BL Lacs with synchrotron X-rays. Our observations of twenty-five of these sources show that their radio morphologies are similar to those of other radio quasars. However, their range of extended powers is more similar to that of BL Lacertae objects (BL Lacs) and extends down to the low values typical of FR I radio galaxies. Five out of our nine lobe-dominated sources have extended radio powers in the range typical of both FR I and FR II radio galaxies, but their extended radio structure is clearly FR II-like. Therefore, we have not yet found a large population of radio quasars hosted by FR Is. Two thirds of our sources have a core-dominated radio morpholgy and thus X-rays likely dominated by the jet. We find that their ratios of radio core to total X-ray luminosity are low and in the regime indicative of synchrotron X-rays. This result shows that also blazars with strong emission lines can produce jets of high-energy synchrotron emission and undermines at least in part the "blazar sequence" scenario which advocates that particle Compton cooling by an external radiation field governs the frequency of the synchrotron emission peak.

Subject headings: BL Lacertae objects: general - galaxies: active - quasars: general - radio continuum: galaxies

1. Introduction

Blazars are one of the most extreme classes of active galactic nuclei (AGN). Their broad-band emission extends from radio up to gama-ray frequencies, varies rapidly and irregularly, is strongly polarized, and shows a core-dominated morphology. Furthermore, apparent superluminal component speeds are often observed in these sources. The properties of blazars can be best explained if we assume that, in fact, they are classical double-lobed radio galaxies with their jets seen at small angles relative to our line of sight and so subject to strong relativistic beaming [see Urry & Padovani (1995) for a review].

Based on their optical spectra, blazars are currently separated into BL Lacertae objects (BL Lacs), defined to have no or only very weak emission lines, and flat-spectrum radio quasars (FSRQ), defined to have strong narrow and broad emission lines [but see Landt et al. (2004) for a suggested revision of the blazar classification scheme]. Within the framework of unified schemes, BL Lacs are identified primarily with beamed low-power Fanaroff-Riley type I (FR I; Fanaroff & Riley 1974) radio galaxies, whereas the high-luminosity Fanaroff-Riley type II (FR II) radio galaxies are assumed to constitute the

parent population of radio quasars.

Traditionally, BL Lacs were discovered in radio and X-ray surveys, and in recent years more efficiently through joint radio-X-ray selections, whereas radio quasars had only been looked for in radio surveys. Thus, it is not surprising that the synchrotron emission of BL Lac jets was found to have its maximum within a wide range of frequencies, from IR/optical to UV/soft-X-ray energies, whereas only radio quasars with synchrotron emission maxima at relatively low energies, and thus X-rays dominated by inverse Compton emission, were known. This, in fact, led to the so-called "blazar sequence" which proposed that the stronger the particle Compton cooling by an external radiation field (such as the one produced by, e.g., the accretion disk or broad emission line region, both stronger in quasars), the lower the frequency of the synchrotron emission peak (Sambruna et al. 1996; Fossati et al. 1998; Ghisellini et al. 1998). In other words, radio quasars with X-rays dominated by synchrotron emission were not expected to exist.

Two recent surveys have drastically changed our picture of blazar jet physics. About 10% of the FSRQ discovered in the Deep X-ray Radio Blazar Survey (DXRBS; Perlman et al. 1998; Landt et al. 2001) and $\sim 30\%$ of the ones identified in the *ROSAT* All-Sky Survey (RASS) - Green Bank (RGB; Laurent-Muehleisen et al. 1998, 1999) have been shown to have spectral energy distributions (SEDs) and broad-band emission properties similar to those of high-energy peaked BL Lacs (Padovani et al. 2003). Subsequent investigations of the *EINSTEIN* Medium Sensitivity Survey (EMSS) and the Slew survey proved that these "X-ray-strong" FSRQ had indeed gone undetected in previous surveys (Wolter & Celotti 2001; Perlman et al. 2001).

In this paper we present the first deep radio interferometric observations of this new class of blazars (Sections 2 and 3) and discuss in the light of our observational results their nature and their relation to "standard" FSRQ and BL Lacs (Section 4). Our conclusions are presented in Section 5. For consistency with previous work we have assumed throughout this paper cosmological parameters $H_0 = 50$ km s^{-1} Mpc^{-1} and $q_0 = 0$. Spectral indices have been defined as $S_\nu \propto \nu^{-\alpha}$.

2. Observations and Data Reduction

We have selected for observations with the NRAO[1] Very Large Array (VLA) flat-spectrum ($\alpha_{\rm r} \lesssim 0.5$) radio quasars from the DXRBS and RGB surveys with radio-to-X-ray spectral indices $\alpha_{\rm rx} \lesssim 0.78$. The latter constraint makes it likely that our sources have their X-rays dominated by synchrotron rather than inverse Compton emission (Padovani & Giommi 1996). We have preferably chosen sources at redshifts $z \lesssim 1$ in order to minimize the effects of surface brightness dimming (Perlman & Stocke 1993) and to increase the probability of detecting large-scale extended radio emission.

We were granted observing time for 25 sources. Their general properties and log of observations are listed in Table 1. The columns are: (1) object name; (2) redshift; (3) total radio flux at 1.4 GHz from the NRAO/VLA Sky Survey (NVSS); (4) radio spectral index between 1.4 and 5 GHz, calculated from the sum of the fluxes of all NVSS sources within a $3'$ radius (corresponding roughly to the beam size of the GB6 survey) and the total flux from the GB6 and PMN surveys for northern and southern sources, respectively; (5) unabsorbed *ROSAT* X-ray flux at 1 keV, calculated using an X-ray spectral index derived from hardness ratios; (6) k-corrected radio-to-X-ray spectral index between 5 GHz and 1 keV; (7) observation date; (8) VLA configuration; and (9) program number. The observed sample contains 19/85 (or 22%) low-redshift ($z \lesssim 1$) FSRQ with $\alpha_{\rm rx} \lesssim 0.78$ from the combined RGB and DXRBS samples. We expect the properties of the observed sources to be representative of this entire subsample, since their total radio and X-ray luminosities span similar ranges.

We observed with the VLA at 1.425 GHz in continuum mode. We imaged all sources with the VLA in A configuration, and were able to gain C array images for 14 of the 25 sources. Three or four scans of several minutes length yielding a total exposure time of ~ 45 minutes were interleaved with one minute scans on a suitable secondary VLA flux calibrator for each source. Scans were spaced to optimize coverage in the (u, v) plane. Multiple ob-

[1]The National Radio Astronomy Observatory is a facility of the National Science Foundation operated under cooperative agreement by Associated Universities, Inc.

servations of 3C 48, 3C 147, or 3C 286 were used to flux-calibrate the maps.

The data were processed with the Astronomical Image Processing System (AIPS; version 31DEC03) package. A model based on Clean components was used to start the self-calibration process. Phase-only self-calibration was used for the first three iterations and amplitude and phase self-calibration for the last one or two iterations. The task IMAGR with robust weighting (ROBUST=0.5) was used to generate the maps and Clean components. We found it useful to combine the self-calibrated data sets from the A and C arrays in order to increase the sensitivity and to improve the (u, v) plane coverage in only 4/14 cases. Our results are shown in Figure 1 and the corresponding map parameters are listed in Table 2, where the columns are as follows: (1) object name; (2) VLA configuration; (3) beam size; (4) position angle; (5) image rms; (6) peak flux; and (7) corresponding panel in Figure 1. The dynamic ranges (peak/noise) of the maps lie between $\sim 100 - 5000$.

The high spatial resolution provided by the A array data allowed a good measure of the core emission, and thus in combination with the C array data an accurate determination of the extended emission flux density, morphology and size. In Table 3 we list the radio properties of the sources as derived from our observations. The columns are: (1) object name; (2) and (3) position of the unresolved core, measured on A array map before start of self-calibration process; (4) core flux density, measured on final A array map; (5) extended flux density, derived from the total flux density measured on C array map (where available and if the source was resolved, else measured on A array map) substracting the core flux density given in column (4); (6) core luminosity k-corrected with spectral index $\alpha_{\rm r} = 0$; (7) extended luminosity k-corrected with spectral index $\alpha_{\rm r} = 0.8$; (8) radio core dominance parameter R, defined as $R = L_{\rm core}/L_{\rm ext}$, where $L_{\rm core}$ and $L_{\rm ext}$ are the core and extended luminosities, respectively; (9) ratio of NVSS flux to total flux density measured on C array map (where available, else measured on A array map); and (10) largest angular extent (LAS), measured from the core to the peak in the extended radio structure [following Murphy et al. (1993)] on C array map (where available, else on A array map). We give 1σ errors and 2σ upper limits. The errors in the core flux densities are on average ~ 0.07 mJy, close to the expected thermal noise. The cumulative errors in the extended flux densities depend upon the solid angular extent of the measured flux. For a considerable number of our sources (11/25 objects) we have only A array data available, which might miss extended flux. We have assessed this effect by using the distribution of values in column (6), i.e., the ratio of NVSS flux to total flux density measured. This has a median of 1.02 and $\sigma = 0.21$. Based on this we have assumed the NVSS flux as the correct total flux for sources with ratios $\gtrsim 1.5$ (the median value plus 2σ). This applies to only one source, namely WGAJ0435−0811, for which we list in column (5) the 'corrected' extended flux.

3. Discussion of Individual Sources

We give now for the individual sources a brief discussion of their general properties and a description of the radio images.

RGB J0112+3818. − An optical spectrum of this source was published in Laurent-Muehleisen et al. (1998) based on which it was classified as a quasar. This source is also part of the CLASS blazar survey (Marchã et al. 2001; Caccianiga et al. 2002). Faint extended radio emission is visible in both images, and most pronounced in the A array image which shows two faint lobes close to the core (Fig. 1(a)).

RGB J0141+3923. − Spectroscopic observations were published in Marziani et al. (2003). This source is also part of the CLASS blazar survey (Marchã et al. 2001; Caccianiga et al. 2002). The source remains unresolved in the radio on the scales imaged (Fig. 1(b)).

RGB J0254+3931. − Optical spectra can be found in Marchã et al. (1996) and Laurent-Muehleisen et al. (1998) who classified this source as a broad-line radio galaxy and quasar respectively. This source shows a one-sided jet on the combined A+C image which is most prominent on the A array image and appears to end in a lobe or hot spot (Figs. 1 (c) and (d)). A similar morphology is visible also on the map published by Taylor et al. (1996) based on VLA B array

snapshot observations at 4.535 GHz.

RGB J1629+4008. − An optical spectrum of this source was published in Laurent-Muehleisen et al. (1998) who classified it as a broad-line radio galaxy based on an absolute optical magnitude of $M > -22$ mag. X-ray observations of this source were obtained with *Beppo*SAX by Padovani et al. (2002). The source remains unresolved in the radio on the scales imaged (Fig. 1(e)). Similarly, the VLA B array map from the FIRST survey at 20 cm shows only an unresolved core.

RGB J2229+3057. − Laurent-Muehleisen et al. (1998) presented an optical spectrum of this source and classified it as a quasar. The source is extended on both A and C array images (Figs. 1(f) and (g)). In particular, on the A array image two well-defined lobes are visible at each side of the nucleus, the closest lobe being fairly extended with a hot spot.

RGB J2256+2618. − An optical spectrum of this source was published by Laurent-Muehleisen et al. (1998) who classified it as a broad-line radio galaxy based on an absolute optical magnitude of $M > -22$ mag. Extended emission on scales of several tens of arcseconds is detected in the C array image (Fig. 1(h)).

RGB J2308+2008. − An optical spectrum can be found in Laurent-Muehleisen et al. (1998). Based on this and an absolute optical magnitude of $M > -22$ mag these authors classified this source as a broad-line radio galaxy. Falco et al. (1998) give a slightly different redshift for this source of $z = 0.2342$ based on four emission lines. The source is unresolved on C array scales, however, a faint lobe is visible close to the core on the A array image (Fig. 1(i)).

RGB J2318+3048. − Laurent-Muehleisen et al. (1998) published an optical spectrum of this source and classified it as a broad-line radio galaxy based on an absolute optical magnitude of $M > -22$ mag. This source is clearly extended on the C array image (Fig. 1(j)), however, only the core is detected on A array scales.

WGA J0106−1034. − Optical spectra of this source can be found in Wolter et al. (1998) and Landt et al. (2001) who classify it as a broad-emission line AGN and quasar, respectively. This source is also part of the FIRST Bright Quasar Survey (Becker et al. 2001) and the Sloan Digital Sky Survey (Schneider et al. 2003). The A array image of this source (Fig. 1(k)) shows extended emission with hot spots on each side of the nucleus, making it clearly an FR II source. However, one of the two hot spots is considerably stronger than the other, and this source appears unusual in that the radio jet we see points towards the weaker of the two lobes. The source is unresolved on C array scales. Our ATCA snapshot observations of this source give a steeper spectral index of $\alpha_{\rm r} = 0.67$ (between 4.8 and 8.6 GHz) than the one listed in Table 1 ($\alpha_{\rm r} = 0.35$).

WGA J0110−1647. − Optical spectra of this source can be found in Perlman et al. (1998) and Caccianiga et al. (2000) who classify it as a quasar and broad-line object, respectively. An extended jet-like feature is clearly visible on the A array image (Fig. 1(l)) a few arcseconds away from the core.

WGA J0126−0500. − An optical spectrum of this source was published by Landt et al. (2001) who classify it as a quasar. The A array image (Fig. 1(m)) shows it to be a double-lobed source with some extended emission also around the core.

WGA J0227−0847. − An optical spectrum of this source can be found in Landt et al. (2001) who classify it as a quasar. This source is also part of the Sloan Digital Sky Survey (Schneider et al. 2003). Our ATCA snapshot observations of this source give a spectral index of $\alpha_{\rm r} = 0.37$ between 4.8 and 8.6 GHz, which is steeper than the one listed in Table 1 ($\alpha_{\rm r} = -0.34$). This is either due to variability or to the fact that this source is a Gigahertz peaked-spectrum (GPS) candidate (e.g., O'Dea 1998). The source remains unresolved in the radio on the scales imaged (Fig. 1(n)). Similarly, the VLA B array map from the FIRST survey at 20 cm shows only an unresolved core.

WGA J0259+1926. − An optical spectrum of this source can be found in Caccianiga et al. (2000) who classify it as a broad-line object. Our own high-quality spectrum of this source will be published shortly. We classify this source as a quasar. The A array image of this source (Fig. 1(o)) shows a jet-like feature extending a few arcseconds away from the core. A slightly extended morphology is visible even on the scales imaged with the VLBA

at 8.4 GHz (Ojha et al. 2004).

WGA J0304+0002. – Optical spectra of this source were published by Perlman et al. (1998) and Caccianiga et al. (2000) who classified it as a quasar and a broad-line object, respectively. This source is also part of the Sloan Digital Sky Survey (Schneider et al. 2003). The source appears extended on both the A and C array images (Fig. 1(p) and (q)) with two well-defined lobes on each side of the nucleus and some fuzzy extended emission on larger scales off one of the lobes. Our ATCA snapshot observations of this source give a steeper spectral index of $\alpha_{\rm r} = 0.71$ (between 4.8 and 8.6 GHz) than the one listed in Table 1 ($\alpha_{\rm r} = 0.40$).

WGA J0435−0811. – Perlman et al. (1998) published an optical spectrum and classified this source as a quasar. It is unresolved on A array scales (Fig. 1(r)), however, most likely its extended emission is resolved out. The NVSS image is slightly extended and the ratio of NVSS to total measured flux on our image for this source is the highest in the sample (see Table 4.2, column (6)).

WGA J0447−0322. – Optical spectra of this source can be found in Perlman et al. (1998) and Caccianiga et al. (2000) who classified it as a quasar and broad-line object, respectively. This source remains unresolved on the scales imaged (Fig. 1(s)). Our ATCA snapshot observations give a steeper spectral index of $\alpha_{\rm r} = 0.91$ (between 4.8 and 8.6 GHz) than the one listed in Table 1 ($\alpha_{\rm r} = 0.47$).

WGA J0544−2241. – Perlman et al. (1998) published an optical spectrum and classified this source as a quasar. The source remains unresolved in the radio on the scales imaged (Fig. 1(t)). Our ATCA snapshot observations give a spectral index of $\alpha_{\rm r} = 0.31$ (between 4.8 and 8.6 GHz), which is steeper than the one listed in Table 1 ($\alpha_{\rm r} = -0.44$). This is either due to variability or to the fact that this source is a Gigahertz peaked-spectrum (GPS) candidate (e.g., O'Dea 1998).

WGA J1026+6746. – Landt et al. (2001) published an optical spectrum and classified this source as a quasar. The A array image (Fig. 1(u)) shows jet-like extended structure over several tens of arcseconds emerging from the core to both sides and an extended lobe to the far left.

WGA J1457−2818. – An optical spectrum of this source can be found in Landt et al. (2001) who classify it as a quasar. Slightly extended emission away from the core is visible on A array scales (Fig. 1(v)). In better accordance with the observed morphology, our ATCA snapshot observations of this source give a steeper spectral index of $\alpha_{\rm r} = 0.72$ (between 4.8 and 8.6 GHz) than the one listed in Table 1 ($\alpha_{\rm r} = 0.40$).

WGA J2239−0631. – Landt et al. (2001) published an optical spectrum and classified this source as a quasar. The source is extended on the C array image (Fig. 1(w)) with two lobes to each side of the nucleus, one of them having a stronger hot spot than the other. Only the nucleus is detected on A array scales.

WGA J2320+0032. – An optical spectrum of this source can be found in Landt et al. (2001) who classify it as a quasar. This source is also part of the Sloan Digital Sky Survey (Schneider et al. 2003). The source remains unresolved in the radio on the scales imaged (Fig. 1(x)). Similarly, the VLA B array map from the FIRST survey at 20 cm shows only an unresolved core.

WGA J2322+2114. – Optical spectra of this source can be found in Wolter et al. (1998) and Perlman et al. (1998) who classify it as a broad-emission line AGN and quasar, respectively. The A array image (Fig. 1(y)) shows clearly a double-lobed structure and a pronounced core.

WGA J2347+0852. – Perlman et al. (1998) published an optical spectrum of this source and classified it as a quasar. This source is extended in both our A and C array images (Figs. 1(z) and (aa)). The X-shape of the galaxy is apparent only in the C array image, whereas on A array scales we observe a central core with two almost equidistant lobes. Both lobes have hot spots, however, one lobe is brighter than the other.

PKS 0256−005. – The optical spectra of this source presented by Richstone et al. (1980) and Osmer et al. (1994) show several strong broad emission lines. This source is also part of the FIRST Bright Quasar Survey (Becker et al. 2001) and the Sloan Digital Sky Survey (Schneider et al. 2003). The source remains unresolved in the radio on the scales imaged (Fig. 1(ab)). Similarly, the

VLA B array map from the FIRST survey at 20 cm shows only an unresolved core.

0959+68W1. − Optical spectra of this source are available from the *Hubble Space Telescope* archive. These show several broad emission lines. This source is also part of the CLASS blazar survey (Marchã et al. 2001; Caccianiga et al. 2002). The A array map (Fig. 1(ac)) shows jet-like features and jet blobs extending over several tens of arcseconds on both sides of the pronounced core.

4. Results and Discussion

In this section we want to address three main questions: 1. How do the general radio properties of these newly discovered strong-lined blazars compare to those of "classical" radio quasars and BL Lacs? 2. Which type of radio galaxies form their parent population? and 3. Is the X-ray emission of these "X-ray strong" radio quasars dominated by the jet and synchrotron in origin?

4.1. The Comparison Samples

For our studies we have selected for comparison other types of radio-loud AGN, namely, steep-spectrum radio quasars (SSRQ), "standard" FSRQ and BL Lacs.

The comparison sample of SSRQ has been drawn from the Molonglo Quasar Sample (MQS) excluding compact steep-spectrum (CSS) quasars and GHz-peaked sources (74 objects). Kapahi et al. (1998) published for this sample total and core radio fluxes, largest angular sizes, and radio spectral indices (between 0.4 and 5 GHz) from observations with the VLA in BnA and CnB configurations at 1.4, 5, and 8.4 GHz, and with the Parkes-Tidbinbilla Interferometer (PTI) at 2.3 GHz. Largest angular sizes were measured between the brightest peaks in the extended radio structure. Improved *ROSAT* X-ray fluxes were published by Baker et al. (1995).

The comparison sample of FSRQ has been selected from the list of Murphy et al. (1993). These authors published core and extended radio fluxes and largest angular sizes for 56 sources from the 1 Jy catalogue (Kühr et al. 1981) as obtained from observations with the VLA in A and B configurations at 1.4 GHz. The largest angular sizes were measured from the core to the peak in the extended radio structure. We have compiled X-ray fluxes at 1 keV and radio spectral indices between 1.4 and 5 GHz for these sources from the multiwavelength catalogue of Padovani et al. (1997).

Additionally, we have chosen for comparison the well-known 1 Jy and EMSS BL Lac samples, since these have complete dedicated VLA observations (e.g., Perlman & Stocke 1993; Cassaro et al. 1999; Rector et al. 2000; Rector & Stocke 2001) as well as in depth *ROSAT* observations (e.g., Perlman et al. 1996; Urry et al. 1996; Rector et al. 1999) available. Perlman & Stocke (1993) give for the EMSS sample largest linear sizes defined as the sum of two straight lines from the core to the outermost 3σ contours, with each line intersecting the brightest hotspot, if any, in the extended structure. Simultaneous radio spectral indices between 1.4 and 5 GHz for this sample have been taken from Cavallotti et al. (2004). Rector & Stocke (2001) give for the 1 Jy sample largest linear sizes defined as in Perlman & Stocke (1993). Radio spectral indices between 2.7 and 5 GHz for this sample have been taken from Stickel et al. (1993).

We have transformed core and extended radio fluxes to 1.4 GHz using a radio spectral index of $\alpha_{\rm r} = 0$ and 0.8, respectively. These same indices have been used to k-correct the luminosities. We have transformed band fluxes to an energy of 1 keV and k-corrected the corresponding luminosities using an X-ray spectral index of $\alpha_{\rm x} = 1.2$.

4.2. The Radio Properties

In this section we investigate the radio properties of the newly discovered "X-ray strong" radio quasars and compare them to those of "classical" radio quasars and BL Lacs.

4.2.1. Extended Radio Powers and the Radio Core Dominance Parameter

In Fig. 2 we have plotted for our sources and the comparison samples introduced in Section 4.1 the extended radio power at 1.4 GHz versus the radio core dominance parameter at this frequency. The extended radio power is believed to be radiated isotropically and, therefore, unaffected by relativistic beaming. Thus this quantity is a good measure of the source's intrinsic jet power. Also marked (horizontal solid lines) are the ranges of extended power typical of FR I and FR II radio

galaxies (Owen & Ledlow 1994). For a constant extended radio power an increase in radio core dominance parameter is indicative of stronger relativistic beaming, since beaming affects only the core emission. For this reason the radio core dominance parameter R is assumed to be a suitable orientation indicator (the higher R, the smaller the viewing angle, i.e., the angle between jet and observer's line of sight).

Fig. 2 shows that, as expected, "classical" radio quasars (SSRQ and FSRQ, filled triangles and squares, respectively) have FR II-like extended powers, with only one FSRQ from the sample of Murphy et al. (1993) having an extended power more typical of an FR I. On the other hand, the BL Lacs from the samples considered here span a range in extended power larger than that of quasars, populating both the FR I- and FR II-regimes. Our sources differ from the radio quasars plotted here. Their range of intrinsic radio power is similar to that of BL Lacs and extends down to the values typical of FR Is, reaching about three orders of magnitude lower values than "classical" radio quasars.

The low radio powers of our sources are partly due to the fact that they are selected from surveys with factors of $\sim 20 - 80$ lower radio flux limits than the comparison radio quasars. This selection, however, gives us a most important result. We have found either the lowest luminosity examples of FR II radio galaxies or quasars hosted by FR Is. The first possibility would indicate that morphology and intrinsic radio power of radio galaxies are not as tightly connected as first found by Fanaroff & Riley (1974). The second possibility would mean that FR I radio galaxies can host quasar nuclei, i.e., they can have broad emission line regions at their centers. To our knowledge, so far only three such objects are known, J2114+820, a broad-line radio galaxy (Lara et al. 1999), E1821+643, a quasar associated with a subarcsecond jet in an FR I radio structure (Blundell & Rawlings 2001), and the well-known FR I broad-line radio galaxy 3C 120 (e.g., Walker et al. 1987). In any case, our finding of a large number of radio quasars with strong emission lines but relatively low radio powers can be regarded as another observational fact against a close relationship between emission line luminosity and jet power in AGN (Rawlings & Saunders 1991), in addition to the existence of radio-quiet quasars (i.e., sources with strong emission lines but extremely weak radio jets) and BL Lacs (i.e., sources with very weak emission lines but strong radio jets).

Fig. 2 also shows that our sources with extended powers in the range populated by the comparison radio quasars have R values intermediate between those of SSRQ and FSRQ. This result, however, does not mean that "X-ray strong" quasars *are* the less beamed versions of "classical" FSRQ. For a correct interpretation we need to take the above mentioned selection effects into account. FSRQ selected in surveys with lower radio flux limits (such as our sources) will have on average lower *total* radio luminosities than FSRQ selected in surveys with higher radio flux limits. Then, considering only a narrow range, i.e., an almost constant value, of relatively high *extended* radio powers, the former will have on average lower *core* luminosities and so will appear less beamed than the latter. In fact, the sources in our sample reach higher R values than the FSRQ in the comparison sample, but at lower extended radio powers.

4.2.2. Largest Linear Sizes

In Fig. 3 we have plotted for our sources and the comparison samples introduced in Section 4.1 the largest linear size (LLS) versus the radio core dominance parameter R at 1.4 GHz. We note that the largest linear sizes were measured differently in each sample. In the FSRQ and our sources they were measured from the core to the peak in the extended structure, whereas in the SSRQ and BL Lac samples they were measured between the peaks of the extended structure on either side of the nucleus. However, we did not attempt to correct the values for the SSRQ and BL Lacs since, on the one hand, such a correction is not straightforward (e.g., assumptions about the intrinsic radio structure are required) and, on the other hand, we are interested mainly in comparisons between our sources and the FSRQ.

As expected from unified schemes, Fig. 3 shows that the largest linear sizes of radio-loud AGN decrease with increasing radio core dominance parameter, i.e., with decreasing angle between jet and observer's line of sight. Our sources follow this trend very well. Significant LLS $-R$ correlations have been reported previously by other authors

for radio quasars, but not for BL Lacs (e.g., Hine & Scheuer 1980; Kapahi & Saikia 1982; Hough & Readhead 1989; Hough et al. 1999). Following their example we plot in Fig. 3 also the relation between LLS and R expected from relativistic beaming models (dashed, dotted and solid lines). In view of the selection effects and incompleteness in the data we restrict ourselves to a prediction of the expected upper and lower envelopes and do not attempt to extract an average or median value of LLS as a function of R to test beaming models.

The fits were obtained as follows. If θ is the angle between the jet axis and the line of sight, the observed values of LLS and R are given by, LLS $= L_0 \sin\theta$ and $R = (R_{90}B(\theta))/2$, where L_0 is the intrinsic largest linear size, R_{90} the radio core dominance parameter that would be observed if the source was oriented at $\theta = 90°$, and $B(\theta) = (1-\beta\cos\theta)^{-(2+\alpha_r)}+(1+\beta\cos\theta)^{-(2+\alpha_r)}$ for the case of a continuous jet with $\beta = v/c$, the ratio of jet velocity to the speed of light. The relation between LLS and R results from their common dependence on viewing angle and its simulation requires initial values for L_0, R_{90}, the Lorentz factor $\Gamma = 1/\sqrt{1-\beta^2}$, and the radio spectral index α_r.

For the radio spectral index we have assumed in all cases a value of $\alpha_r = 0.8$, which is typical of optically thin synchrotron emission. Radio galaxies can have different intrinsic radio core dominance values and we have assumed values of $R_{90} = 0.022$ and 0.003, the median values obtained by Morganti et al. (1997) for their samples of FR I and narrow line FR II radio galaxies, respectively. In the case of $R_{90} = 0.003$, the upper and lower envelopes in Fig. 3 can be fitted if we assume a bulk Lorentz factor of $\Gamma = 8$ and values of $L_0 = 1900$ and 30 kpc, respectively (dashed lines). In the case of $R_{90} = 0.022$, a slightly lower bulk Lorentz factor of $\Gamma = 6$ and values of $L_0 = 1400$ and 20 kpc, respectively, are required (dotted lines). We note that a fit with a lower radio spectral index would require a much higher value of the bulk Lorentz factor, e.g., in the case of $\alpha_r = 0.2$ and $R_{90} = 0.003$ a value of $\Gamma = 15$.

Previously presented LLS $-$ R relations included only lobe-dominated radio quasars, i.e., sources viewed at relatively large angles, but did not account for this by restricting the range of orientation accordingly. Thus it is not suprising that fits to their envelopes required smaller Lorentz factors of $\Gamma = 2-5$ (for values of R_{90} similar to our FR II radio galaxy case). We note also that the sources in the samples considered here reach higher LLS values than those included in the previous studies. We have included in Fig. 3 both quasars and BL Lacs and it appears that they follow the same relation, but their starting points are most probably different, which we have accounted for here by adopting two cases of R_{90}. The resulting maximum intrinsic LLS values of their parent radio galaxies are not very much different and in accordance with the result of Ledlow et al. (2002) who found maximum sizes for both FR I and FR II radio galaxies around 2000 kpc (with only one source exceding this value).

4.2.3. The Selection of Blazars

Past and on-going blazar surveys, such as, e.g., the 1 Jy BL Lac survey (Stickel et al. 1991), CLASS blazar survey (Marchã et al. 2001; Caccianiga et al. 2002) and DXRBS (Perlman et al. 1998; Landt et al. 2001), have selected their candidates based on radio spectral index. A limit of $\alpha_r = 0.5$ is generally chosen, since radio sources are expected to become increasingly core-dominated below this value (Orr & Browne 1982). Ideally, blazar selection should be based on orientation, but methods to derive actual viewing angles require long-term radio observations and/or sophisticated multiwavelength data sets. A blazar selection based on the value of the radio core dominance parameter of $R > 1$ would then be another possibility, but this would require dedicated radio observations for a large number of sources, which are usually not readily available. Therefore, this approach would be extremely time consuming.

In order to assess the effect of blazar selection based on radio spectral index relative to one possibly based on the radio core dominance parameter we have plotted in Fig. 4 for our sources and the samples introduced in Section 4.1 these two quantities versus each other. Fig. 4 shows that indeed radio-loud AGN appear to populate preferably the regions of either steep radio spectral index ($\alpha_r > 0.5$) and lobe-dominance (i.e., $R < 1$) or flat radio spectral index ($\alpha_r < 0.5$) and core-dominance (i.e., $R > 1$). Only a few sources in blazar surveys imposing a radio spectral index cut of $\alpha_r = 0.5$ are expected to be lobe-dominated,

and similarly, only a few core-dominated sources are expected to be missed by these surveys.

A considerable fraction of our sources (7/25 or 28%), however, have a flat radio spectral index $\alpha_{\rm r} \leq 0.5$ and *are* lobe-dominated. Are we then justified to refer to these sources as blazars? Variability undoubtedly plays a role in the explanation of the existence of at least some of the lobe-dominated flat-spectrum radio sources, however, it is unlikely that it can account for the existence of all of them. For example, we have additional ATCA snapshot observations available for 3 out of the 7 sources, and for two of them, namely, WGAJ0106−1034 and WGAJ0304+0002, these yield steep radio spectral indices of $\alpha_{\rm r} = 0.67$ and 0.71, respectively. For WGAJ0126−0500 our ATCA observations give $\alpha_{\rm r} = 0.39$, only slightly steeper than the value of 0.21 listed in Table 1. A more plausible explanation for the existence of lobe-dominated flat-spectrum radio sources can instead be gained from simulations of the relation between $\alpha_{\rm r}$ and R.

From the definitions of the radio spectral index between two frequencies ν_1 and ν_2 of $(S_{\nu_1}/S_{\nu_2}) \propto (\nu_1/\nu_2)^{-\alpha_{\rm r}}$ and the relation between the radio core dominance parameters at these two frequencies of $R_{\nu_2} = R_{\nu_1}(\nu_1/\nu_2)^{\alpha_{\rm r_c}-\alpha_{\rm r_e}}$, where $\alpha_{\rm r_c}$ and $\alpha_{\rm r_e}$ are the radio spectral indices of the core and extended radio emission, respectively, we have derived $\alpha_{\rm r} - \log R_{\nu_1}$ relations for different values of $\alpha_{\rm r_c}$. We have assumed for ν_1 and ν_2 values of 1.4 and 5 GHz, respectively, and for the extended emission a radio spectral index of $\alpha_{\rm r_e} = 0.8$. Our results are shown in Fig. 4 as dashed lines from top to bottom for a core radio spectral index of $\alpha_{\rm r_c} = 0.5$, 0, −0.5, and −1.3.

Firstly, we note that the relation between $\alpha_{\rm r}$ and $\log R$ is not a linear one (see also Kembhavi et al. 1986), contrary to what the fit of Cavallotti et al. (2004) to their Fig. 4 suggests. Secondly, our results show that lobe-dominated flat-spectrum radio sources can indeed exist, if the core emission has a radio spectral index of $\alpha_{\rm r_c} \lesssim 0$. In general, the lower the core radio spectral index, the less core flux relative to the extended emission is required to render the total radio spectral index of the source below a value of $\alpha_{\rm r_c} = 0.5$. Therefore, a blazar selection and definition based on a radio core dominance parameter value of $R \gtrsim 1$ appears to be more robust than one based on a radio spectral index of $\alpha_{\rm r} \lesssim 0.5$. But, as Fig. 4 shows, a selection based on a flat radio spectral index is expected to include lobe-dominated sources rather than to miss blazars.

In this regard, we note that the result that FR I radio galaxies have higher R values than FR II radio galaxies (e.g., Morganti et al. 1997) could be due to selection effects. If the cores of FR II radio galaxies had on average lower radio spectral indices than the ones of FR I radio galaxies, in samples selecting at relatively high frequencies and thus sensitive to flat-spectrum sources, the first will appear on average less core-dominated than the latter.

4.3. The Parent Population

According to current unified schemes for radio-loud AGN, weak-lined blazars, the BL Lacs, are harboured mainly by low-power radio galaxies, the FR Is, whereas radio quasars are hosted by high-luminosity FR II radio galaxies. In Section 4.2 we have shown that our sources extend the range of intrinsic radio powers of quasars down to the low values typical of FR Is and BL Lacs. What then is the parent population of our newly discovered "X-ray strong" radio quasars?

In our sample, 9/25 sources are lobe-dominated and in principle a morphological classification of their extended radio structure is possible. Out of these, 4 sources have FR II-like extended radio powers with two of them, WGAJ0106−1034 and WGAJ2322+2114, having also a clear FR II-like morphology. They show extended lobes with prominent hot spots in their outer regions. The morphology of WGAJ0304+0002 is not clear. One of the lobes appears to have an outer hot spot and so is indicative of an FR II. The other lobe, however, might be more FR I-like. A higher quality map of this object would be helpful in this case. The source WGAJ1026+6746 shows an extended jet structure with some extended lobe emission. We tentatively interpret its morphology as FR II-like. Another 5 sources have extended radio powers typical of both FR Is and FR IIs. Out of these, RGBJ2229+3057, WGAJ0126−0500, and WGAJ2347+0852 show a clear FR II-like morphology, especially on the A array map. The extended structure of WGAJ2239−0631 appears to be more FR II-like, however, only a B array image can assess this with certainty. The source

WGAJ0435−0811 needs to be imaged in B or C array in order to classify its extended emission, since this is most likely resolved out on the scales imaged (see Section 2).

Unfortunately, all sources in our sample with extended powers typical of FR Is (8/25 objects) are core-dominated and so a morphological classification of their extended emission is not possible. Sources with extended powers in this low regime and lobe-dominated morphology are the most interesting ones, since they can clarify if a large population of low-luminosity FR II radio galaxies and/or quasars hosted by FR Is exist. In this respect, it is vital to observe with the VLA more "X-ray strong" radio quasars and in general radio quasars with low total radio powers in order to search for this kind of objects.

4.4. The Origin of the X-ray Emission

The X-ray emission of radio-loud AGN, contrary to their emission at radio frequencies, is believed to be made up of at least three components with different origins: an isotropic one, produced by the ambient hot gas (presumably from the group or cluster associated with the source or from the galaxy), and two anisotropic components, one generally interpreted as inverse Compton emission from the accretion disk corona, which is present also in radio-quiet quasars and is expected to be seen only in sources with their nuclei unobscured by the central dusty torus, and the other associated with the powerful relativistic jet and thus subject to beaming.

In order to constrain the origin of the X-ray emission in our sources we have plotted in Fig. 5 their ratio of radio core to total X-ray luminosity versus the radio core dominance parameter R. A plot such as the one displayed in Fig. 5 is most suitable for our purpose. Relativistic beaming is believed to increase only the core jet emission, both radio and X-ray, and leave any isotropically emitted extended emission unaffected. If the total X-ray emission $L_{\rm x}$ is dominated by an unbeamed component, the ratio $L_{\rm core}/L_{\rm x}$ will then increase with R until the beamed jet emission starts to dominate the X-rays. Once this is the case, the ratio $L_{\rm core}/L_{\rm x}$ will stay constant and reflect simply the ratio intrinsic to the jet (assuming that the radio and X-ray beaming parameters are the same).

To investigate if this behaviour is indeed observed we have included for comparison in Fig. 5 also other types of radio-loud AGN, selected as described in Section 4.1. From Fig. 5 we see that, as expected, the X-ray emission in SSRQ (filled triangles), which are lobe-dominated sources and so are presumably seen at larger angles, appears to be dominated by an unbeamed component (Kembhavi 1993; Baker et al. 1995; Siebert et al. 1998). Their ratios of radio core emission to total X-ray luminosity $L_{\rm core}/L_{\rm x}$ increase with R. On the other hand, in FSRQ (filled squares), which are core-dominated sources and so are presumably seen at small angles, the X-ray emission appears to be indeed dominated by the beamed jet. Their ratios of $L_{\rm core}/L_{\rm x}$ are independent of R. In these sources these ratios should then reflect the intrinsic jet SED, where values of $\log L_{\rm core}/L_{\rm x} \geq 6$ and < 6 are indicative of X-rays dominated by inverse Compton and synchrotron emission, respectively (Padovani & Giommi 1996).

However, so far, BL Lacs have been the only blazars known to have jets with synchrotron X-rays. This is apparent in Fig. 5 where these sources (open squares), almost all core-dominated, span a large range in $L_{\rm core}/L_{\rm x}$ and reach relatively low values. On the other hand, all but two of the "classical" FSRQ plotted here have ratios of $L_{\rm core}/L_{\rm x} \geq 6$.

What is the origin of the X-ray emission in our newly discovered "X-ray strong" radio quasars? Their distribution in Fig. 5 shows that a third (9/25 objects) fall in the range $R < 1$ and follow the behaviour exhibited by SSRQ. Therefore, the X-ray emission in these sources is most likely *not* dominated by the jet, but comes rather from the ambient hot gas and/or the the accretion disk. We have performed correlation analysis for the following three cases, all SSRQ (63 sources), SSRQ with detected X-ray emission (24 sources), and our lobe-dominated sources. In the first case censored data was present and we used the ASURV analysis package (Isobe et al. 1986). In all cases the observed correlations are highly significant ($P > 99.9\%$) with slopes 0.79 ± 0.11, 0.88 ± 0.09, and 0.93 ± 0.28, respectively, not significantly different from one (as expected for a roughly constant ratio of $L_{\rm ext}/L_{\rm x}$). The best fits are shown as dashed lines in Fig. 5. At $R = 1$, these correlations give the average $\log L_{\rm core}/L_{\rm x}$ ratios intrinsic

to the jets of the corresponding population. Fig. 5 shows that this value is for our sources < 6, i.e., suggestive of synchrotron X-rays.

The majority of our sources (16/25 objects) have a core-dominated radio morphology and, contrary to the majority of "classical" FSRQ, their $L_{\rm core}/L_{\rm x}$ ratios extend well into the region populated by high-energy peaked BL Lacs. In fact, almost all of our core-dominated sources (14/16 objects) have ratios $\log L_{\rm core}/L_{\rm x} \leq 6$, indicative of synchrotron X-rays. The definite proof of the synchrotron nature of their X-ray emission, however, will require X-ray imaging and spectroscopy.

Dedicated X-ray observations exist or have been scheduled for 11/25 sources presented here. RGBJ1629+4008, the core-dominated radio quasar with the lowest $L_{\rm core}/L_{\rm x}$ ratio in our sample, has been observed with *Beppo*SAX by Padovani et al. (2002) and found to have X-rays dominated by synchrotron radiation with a peak frequency $\sim 2{\times}10^{16}$ Hz. A further four sources have been observed with XMM-Newton in AO-3 (PI: Padovani) and six sources have been approved for observation with *Chandra* in Cycle 6 (PI: Landt). Out of these 10 objects, 6 sources are core-dominated and have the lowest $L_{\rm core}/L_{\rm x}$ ratios in our sample after RGBJ1629+4008.

5. Summary and Conclusions

A considerable fraction of flat-spectrum radio quasars discovered in two recent blazar surveys (DXRBS and RGB) have multiwavelength emission properties similar to those of BL Lacs with synchrotron X-rays (Padovani et al. 2003). If it can be shown that these "X-ray loud" radio quasars are indeed the strong-lined version of high-energy peaked BL Lacs, it could mean that jet energetics are less dependent on emission line luminosity than advocated so far (Sambruna et al. 1996; Fossati et al. 1998; Ghisellini et al. 1998).

In this paper we have presented deep VLA radio images obtained at 1.4 GHz in A and C configurations of 25 of these newly discovered blazars (8 RGB and 17 DXRBS sources). We have compared the radio properties of our sources with those of other classes of radio-loud AGN, namely, "classical" steep- and flat-spectrum radio quasars and BL Lacs. Our main results can be summarized as follows.

(i) The radio morphologies of our sources are similar to those generally observed for radio quasars and include prominent cores, lobes and jet features. Their range of extended radio powers, however, is similar to that of BL Lacs and extends down to the values typical of FR I radio galaxies, reaching about three orders of magnitude lower values than "classical" radio quasars. This result is partly due to the fact that our sources are selected from surveys with relatively low radio flux limits.

(ii) In our sample, 9/25 sources are lobe-dominated and in principle a morphological classification of their extended radio structure is possible. Out of these, 4 sources have FR II-like extended powers with two having a clear and another two a tentative FR II-like morphology. Another 5 sources have extended radio powers typical of both FR Is and FR IIs. Out of these, 4 show a clear FR II-like morphology, whereas one source requires further observations since its extended emission is resolved out on the scales imaged.

(iii) As expected from unified schemes, we find for our sources and the comparison samples of radio-loud AGN that the largest linear sizes (LLS) decrease with increasing radio core dominance parameter R. Fits based on the relativistic beaming model to the upper and lower envelopes of the observed LLS$-R$ relation yield bulk Lorentz factors of $\Gamma = 6-8$ and maximum and minimum intrinsic LLS values of ~ 2000 and ~ 20 kpc, respectively.

(iv) The majority of our sources (16/25 objects) have a core-dominated radio morphology and thus their total X-ray emission is expected to be dominated by the jet. Out of these, 14/16 have ratios of radio core to total X-ray luminosity $\log L_{\rm core}/L_{\rm x} \leq 6$, indicative of synchrotron X-rays (Padovani & Giommi 1996). The definite proof of the synchrotron nature of their X-ray emission, however, will require dedicated observations with *Chandra* and XMM-Newton.

We plan to continue our VLA observing program of "X-ray loud" radio quasars in order to find in particular lobe-dominated radio quasars with low extended powers. These sources could then help us clarify if a large population of quasars hosted by FR Is exists.

H.L. acknowledges financial support from the

Deutsche Akademie der Naturforscher Leopoldina grant number BMBF-LPD 9901/8-99. This research has made use of the NASA/IPAC Extragalactic Database (NED) which is operated by the Jet Propulsion Laboratory, California Institute of Technology, under contract with the National Aeronautics and Space Administration.

REFERENCES

Baker, J. C., Hunstead, R. W., & Brinkmann, W. 1995, MNRAS, 277, 553

Becker, R. H., et al. 2001, ApJS, 135, 227

Blundell, K. M., & Rawlings, S. 2001, ApJ, 562, L5

Caccianiga, A., Maccacaro, T., Wolter, A., Della Ceca, R., & Gioia, I. M. 2000, A&AS, 144, 247

Caccianiga, A., Marchã, M. J., Antón, S., Mack, K.-H., & Neeser, M. J. 2002, MNRAS, 329, 877

Cassaro, P., Stanghellini, C., Bondi, M., Dallacasa, D., Della Ceca, R., & Zappalà, R. A. 1999, A&AS, 139, 601

Cavallotti, F., Wolter, A., Stocke, J. T., & Rector, T. 2004, A&A, 419, 459

Falco, E. E., Kochanek, C. S., & Munoz, J. A. 1998, ApJ, 494, 47

Fanaroff, B. L., & Riley, J. M. 1974, MNRAS, 167, 31

Fossati, G., Maraschi, L., Celotti, A., Comastri, A., & Ghisellini, G. 1998, MNRAS, 299, 433

Ghisellini, G., Celotti, A., Fossati, G., Maraschi, L., & Comastri, A. 1998, MNRAS, 301, 451

Hine, R. G., & Scheuer, P. A. G. 1980, MNRAS, 193, 285

Hough, D. H., & Readhead, A. C. S. 1989, AJ, 98, 1208

Hough, D. H., et al. 1999, ApJ, 511, 84

Isobe, T., Feigelson, E. D., & Nelson, P. I. 1986, ApJ, 306, 490

Kapahi, V. K., Athreya, R. M., Subrahmanya, C. R., Baker, J. C., Hunstead, R. W., McCarthy, P. J., & van Breugel, W. 1998, ApJS, 118, 327

Kapahi, V. K., & Saikia, D. J. 1982, JApA, 3, 465

Kembhavi, A. 1993, MNRAS, 264, 683

Kembhavi, A., Feigelson, E. D., & Singh, K. P. 1986, MNRAS, 220, 51

Kühr, H., Witzel, A., Pauliny-Toth, I. I. K., & Nauber, U. 1981, A&AS, 45, 367

Landt, H., Padovani, P., Perlman, E. S., & Giommi, P. 2004, MNRAS, 351, 83

Landt, H., Padovani, P., Perlman, E. S., Giommi, P., Bignall, H., & Tzioumis, A. 2001, MNRAS, 323, 757

Lara, L., Márquez, I., Cotton, W. D., Feretti, L., Giovannini, G., Marcaide, J. M., & Venturi, T. 1999, NewARev, 43, 643

Laurent-Muehleisen, S. A., Kollgaard, R., Feigelson, E. D., Brinkmann, W., & Siebert, J. 1999, ApJ, 525, 127

Laurent-Muehleisen, S. A., Kollgaard, R. I., Ciardullo, R., Feigelson, E. D., Brinkmann, W., & Siebert, J. 1998, ApJS, 118, 127

Ledlow, M. J., Owen, F. N., & Eilek, J. A. 2002, NewAR, 46, 343

Marchã, M. J., Caccianiga, A., Browne, I. W. A., & Jackson, N. 2001, MNRAS, 326, 1455

Marchã, M. J. M., Browne, I. W. A., Impey, C. D., & Smith, P. S. 1996, MNRAS, 281, 425

Marziani, P., Sulentic, J. W., Zamanov, R., Calvani, M., Dultzin-Hacyan, D., Bachev, R., & Zwitter, T. 2003, ApJS, 145, 199

Morganti, R., Oosterloo, T. A., Reynolds, J. E., Tadhunter, C. N., & Migenes, V. 1997, MNRAS, 284, 541

Murphy, D. W., Browne, I. W. A., & Perley, R. A. 1993, MNRAS, 264, 298

O'Dea, C. P. 1998, PASP, 110, 493

Ojha, R., Fey, A. L., Lovell, J. E. J., Jauncey, D. L., & Johnston, K. J. 2004, AJ, 128, 1570

Orr, M. J. L., & Browne, I. W. A. 1982, MNRAS, 200, 1067

Osmer, P. S., Porter, A. C., & Green, R. F. 1994, ApJ, 436, 678

Owen, F. N., & Ledlow, M. J. 1994, in The First Stromlo Symposium: The Physics of Active Galaxies, ed. G. V. Bicknell, M. A. Dopita, & P. J. Quinn (A.S.P., San Francisco), 319

Padovani, P., Costamante, L., Ghisellini, G., Giommi, P., & Perlman, E. S. 2002, ApJ, 581, 895

Padovani, P., & Giommi, P. 1996, MNRAS, 279, 526

Padovani, P., Giommi, P., & Fiore, F. 1997, MmSAI, 68, 147

Padovani, P., Perlman, E. S., Landt, H., Giommi, P., & Perri, M. 2003, ApJ, 588, 128

Perlman, E. S., Padovani, P., Giommi, P., Sambruna, R., Jones, L. R., Tzioumis, A., & Reynolds, J. 1998, AJ, 115, 1253

Perlman, E. S., Padovani, P., Landt, H., Stocke, J. T., Costamante, L., Rector, T., Giommi, P., & Schachter, J. F. 2001, in Blazar Demographics and Physics, ed. P. Padovani & C. M. Urry (A.S.P., San Francisco), 200

Perlman, E. S., & Stocke, J. T. 1993, ApJ, 406, 430

Perlman, E. S., Stocke, J. T., Wang, Q. D., & Morris, S. L. 1996, ApJ, 456, 451

Rawlings, S., & Saunders, R. 1991, Nature, 349, 138

Rector, T. A., & Stocke, J. T. 2001, AJ, 122, 565

Rector, T. A., Stocke, J. T., & Perlman, E. S. 1999, ApJ, 516, 145

Rector, T. A., Stocke, J. T., Perlman, E. S., Morris, S. L., & Gioia, I. M. 2000, AJ, 120, 1626

Richstone, D. O., Ratnatunga, K., & Schaeffer, J. 1980, ApJ, 240, 1

Sambruna, R. M., Maraschi, L., & Urry, C. M. 1996, ApJ, 463, 444

Schneider, D. P., et al. 2003, AJ, 126, 2579

Siebert, J., Brinkmann, W., Drinkwater, M. J., Yuan, W., Francis, P. J., Peterson, B. A., & Webster, R. L. 1998, MNRAS, 301, 261

Stickel, M., Fried, J. W., & Kühr, H. 1993, A&AS, 98, 393

Stickel, M., Padovani, P., Urry, C. M., Fried, J. W., & Kühr, H. 1991, ApJ, 374, 431

Taylor, G. B., Vermeulen, R. C., Readhead, A. C. S., Pearson, T. J., Henstock, D. R., & Wilkinson, P. N. 1996, ApJS, 107, 37

Urry, C. M., & Padovani, P. 1995, PASP, 107, 803

Urry, C. M., Sambruna, R., Worrall, D. M., Kollgaard, R. I., Feigelson, E. D., Perlman, E. S., & Stocke, J. T. 1996, ApJ, 463, 424

Walker, R. C., Benson, J. M., & Unwin, S. C. 1987, ApJ, 316, 546

Wolter, A., & Celotti, A. 2001, A&A, 371, 527

Wolter, A., Ruscica, C., & Caccianiga, A. 1998, MNRAS, 299, 1047

This 2-column preprint was prepared with the AAS LaTeX macros v5.2.

TABLE 1

GENERAL PROPERTIES OF THE SAMPLE AND LOG OF OBSERVATIONS

Object Name	z	$f_{\rm NVSS}$ [mJy]	$\alpha_{\rm r}$	$f_{\rm 1keV}$ [μJy]	$\alpha_{\rm rx}$	observed	Array	program
(1)	(2)	(3)	(4)	(5)	(6)	(7)	(8)	(9)
RGB J0112+3818	0.333	57.5	0.09	0.096	0.72	01/10/2001	A	AP395
						05/01/2000	C	AP395
RGB J0141+3923	0.080	116.5	0.30	0.126	0.75	01/10/2001	A	AP395
						05/01/2000	C	AP395
RGB J0254+3931	0.291	230.4	−0.31	0.344	0.76	01/10/2001	A	AP395
						05/01/2000	C	AP395
RGB J1629+4008	0.272	9.0	−0.29	0.211	0.61	11/14/2000	A	AP395
						05/01/2000	C	AP395
RGB J2229+3057	0.322	150.4	0.15	0.203	0.74	01/10/2001	A	AP395
						05/01/2000	C	AP395
RGB J2256+2618	0.121	43.6	−0.02	0.208	0.69	11/14/2000	A	AP395
						05/01/2000	C	AP395
RGB J2308+2008	0.250	188.4	0.12	0.151	0.77	01/10/2001	A	AP395
						05/01/2000	C	AP395
RGB J2318+3048	0.103	23.1	0.12	0.185	0.65	11/14/2000	A	AP395
						05/01/2000	C	AP395
WGA J0106−1034	0.469	276.0	0.35	0.091	0.79	03/24/2002	A	AL564
						09/12/2005	C	AL652
WGA J0110−1647	0.781	105.6	0.35	0.176	0.69	11/28/2004	A	AP479
WGA J0126−0500	0.411	58.4	0.21	0.076	0.74	11/07/2004	A	AL627
WGA J0227−0847	2.228	65.3	−0.34	0.051	0.70	11/28/2004	A	AP479
WGA J0259+1926	0.544	163.7	0.16	0.089	0.75	03/24/2002	A	AL564
WGA J0304+0002	0.563	123.8	0.40	0.121	0.74	03/24/2002	A	AL564
						09/12/2005	C	AL652
WGA J0435−0811	0.791	50.1	−0.27	0.028	0.75	02/09/2002	A	AL564
WGA J0447−0322	0.774	86.7	0.47	0.348	0.66	02/09/2002	A	AL564
						10/18/2002	C	AL578
WGA J0544−2241	1.537	133.2	−0.44	0.085	0.74	11/02/2004	A	AL627
						10/03/2002	CnB	AL578
WGA J1026+6746	1.181	234.0	0.49	0.069	0.76	11/28/2004	A	AP479
WGA J1457−2818	1.999	225.4	0.40	0.019	0.74	12/04/2004	A	AL627
WGA J2239−0631	0.264	117.2	0.54	0.259	0.69	09/30/2004	A	AL627
						09/12/2005	C	AL652
WGA J2320+0032	1.894	82.0	0.45	0.036	0.76	09/30/2004	A	AL627
WGA J2322+2114	0.707	151.6	0.31	0.064	0.77	09/29/2004	A	AL627
WGA J2347+0852	0.292	147.7	0.58	0.176	0.71	01/10/2001	A	AP395
						05/01/2000	C	AP395
PKS 0256−005	1.995	228.2	−0.59	0.102	0.78	11/28/2004	A	AP479
0959+68W1	0.773	101.9	0.41	0.114	0.75	11/28/2004	A	AP479

TABLE 2
MAP PARAMETERS

Object Name	Array	beam [arcsec]	PA [deg]	rms [mJy/ beam]	peak [mJy/ beam]	Fig. 1
(1)	(2)	(3)	(4)	(5)	(6)	(7)
RGB J0112+3818	A	1.4× 1.3	−60	0.04	32.5	(a)
RGB J0141+3923	A	1.4× 1.3	−52	0.12	104.5	(b)
RGB J0254+3931	A	1.4× 1.3	73	0.08	160.2	(c)
RGB J0254+3931	A+C	6.0× 6.0	85	0.07	167.5	(d)
RGB J1629+4008	A	2.0× 1.3	80	0.04	8.6	(e)
RGB J2229+3057	A	1.4× 1.3	−84	0.04	44.2	(f)
RGB J2229+3057	A+C	7.4× 6.5	49	0.04	44.2	(g)
RGB J2256+2618	C	15.3×14.5	−84	0.06	24.7	(h)
RGB J2308+2008	A	1.6× 1.4	66	0.06	218.0	(i)
RGB J2318+3048	C	15.0×14.4	−90	0.06	22.2	(j)
WGA J0106−1034	A	2.0× 1.3	16	0.03	105.5	(k)
WGA J0110−1647	A	2.0× 1.3	10	0.10	72.0	(l)
WGA J0126−0500	A	1.7× 1.2	12	0.13	14.6	(m)
WGA J0227−0847	A	1.7× 1.3	− 7	0.10	76.7	(n)
WGA J0259+1926	A	1.4× 1.3	27	0.05	133.1	(o)
WGA J0304+0002	A	1.6× 1.4	15	0.03	8.4	(p)
WGA J0304+0002	A+C	6.5× 5.4	51	0.04	29.1	(q)
WGA J0435−0811	A	1.8× 1.4	3	0.04	30.3	(r)
WGA J0447−0322	A	1.6× 1.4	4	0.09	68.0	(s)
WGA J0544−2241	A	2.7× 1.3	−19	0.06	149.6	(t)
WGA J1026+6746	A	2.7× 1.3	−66	0.12	84.7	(u)
WGA J1457−2818	A	2.7× 1.3	− 4	0.16	190.4	(v)
WGA J2239−0631	C	17.8×15.9	3	0.07	52.6	(w)
WGA J2320+0032	A	1.5× 1.4	−14	0.15	65.6	(x)
WGA J2322+2114	A	1.4× 1.2	−53	0.04	40.4	(y)
WGA J2347+0852	A	1.5× 1.4	53	0.06	19.4	(z)
WGA J2347+0852	A+C	8.5× 8.4	−38	0.08	52.3	(aa)
PKS 0256−005	A	1.6× 1.4	−14	0.05	252.1	(ab)
0959+68W1	A	2.6× 1.3	−70	0.06	80.1	(ac)

TABLE 3
OBSERVED 20 CENTIMETER RADIO PROPERTIES OF THE SAMPLE

Object Name (1)	R.A.(J2000) (2)	Decl.(J2000) (3)	$f_{\rm core}$ [mJy] (4)	$f_{\rm ext}$ [mJy] (5)	$\log L_{\rm core}$ [W/Hz] (6)	$\log L_{\rm ext}$ [W/Hz] (7)	$\log R$ (8)	$f_{\rm NVSS}/f_{\rm total}$ (9)	LAS [arcsec] (10)
RGB J0112+3818	01 12 18.049	+38 18 56.90	32.5	5.8±0.4	25.20	24.55	0.65	1.50	20.6
RGB J0141+3923	01 41 57.756	+39 23 29.10	104.5	<0.2	24.46	<21.77	>2.69	1.11	<1.4
RGB J0254+3931	02 54 42.629	+39 31 34.75	160.2	74.4±1.1	25.77	25.53	0.24	0.98	34.4
RGB J1629+4008	16 29 01.336	+40 08 00.10	8.6	<0.2	24.44	<22.89	>1.55	1.05	<2.0
RGB J2229+3057	22 29 34.151	+30 57 12.10	44.2	116.5±0.4	25.30	25.82	−0.52	0.94	90.6
RGB J2256+2618	22 56 39.163	+26 18 43.55	21.4	12.6±0.4	24.13	23.94	0.19	1.28	65.9
RGB J2308+2008	23 08 11.630	+20 08 42.05	218.0	9.7±0.3	25.77	24.50	1.27	0.83	7.1
RGB J2318+3048	23 18 36.905	+30 48 37.00	17.5	12.1±0.4	23.90	23.78	0.12	0.78	41.5
WGA J0106−1034	01 06 44.158	−10 34 10.55	105.5	141.9±0.3	26.02	26.28	−0.26	1.12	9.0
WGA J0110−1647	01 10 35.516	−16 48 27.80	72.0	27.0±0.8	26.31	26.09	0.22	1.07	31.8
WGA J0126−0500	01 26 15.090	−05 01 22.10	14.6	27.8±2.6	25.04	25.44	−0.40	1.38	40.7
WGA J0227−0847	02 27 32.070	−08 48 12.20	76.7	<0.2	27.36	<26.18	>1.18	0.85	<1.3
WGA J0259+1926	02 59 29.650	+19 25 44.35	133.1	11.8±0.3	26.25	25.35	0.90	1.13	8.1
WGA J0304+0002	03 04 58.973	+00 02 35.85	8.4	118.3±0.3	25.08	26.38	−1.30	0.98	42.4
WGA J0435−0811	04 35 08.353	−08 11 02.75	30.3	19.8	25.95	25.97	−0.02	1.65	
WGA J0447−0322	04 47 54.727	−03 22 42.20	68.0	<0.1	26.28	<23.65	>2.63	1.28	<1.6
WGA J0544−2241	05 44 07.560	−22 41 09.85	149.6	<0.1	27.27	<24.42	>2.85	0.89	<2.7
WGA J1026+6746	10 26 33.850	+67 46 12.10	84.7	158.7±1.3	26.77	27.27	−0.50	1.02	44.6
WGA J1457−2818	14 57 44.599	−28 19 21.60	190.4	30.0±0.7	27.64	27.22	0.42	1.02	6.3
WGA J2239−0631	22 39 46.832	−06 31 50.55	46.8	69.1±0.4	25.15	25.40	−0.25	1.01	50.6
WGA J2320+0032	23 20 37.983	+00 31 39.70	65.6	<0.3	27.12	<25.15	>1.97	1.25	<1.5
WGA J2322+2114	23 22 02.607	+21 13 56.45	40.4	86.9±1.1	25.97	26.49	−0.52	1.19	55.9
WGA J2347+0852	23 47 38.144	+08 52 46.35	8.3	136.2±0.8	24.49	25.79	−1.30	1.02	22.3
PKS 0256−005	02 59 28.510	−00 20 00.00	252.2	<0.1	27.76	<24.74	>3.02	0.90	<1.6
0959+68W1	10 03 06.760	+68 13 16.80	80.1	26.8±0.7	26.35	26.07	0.28	0.95	27.6

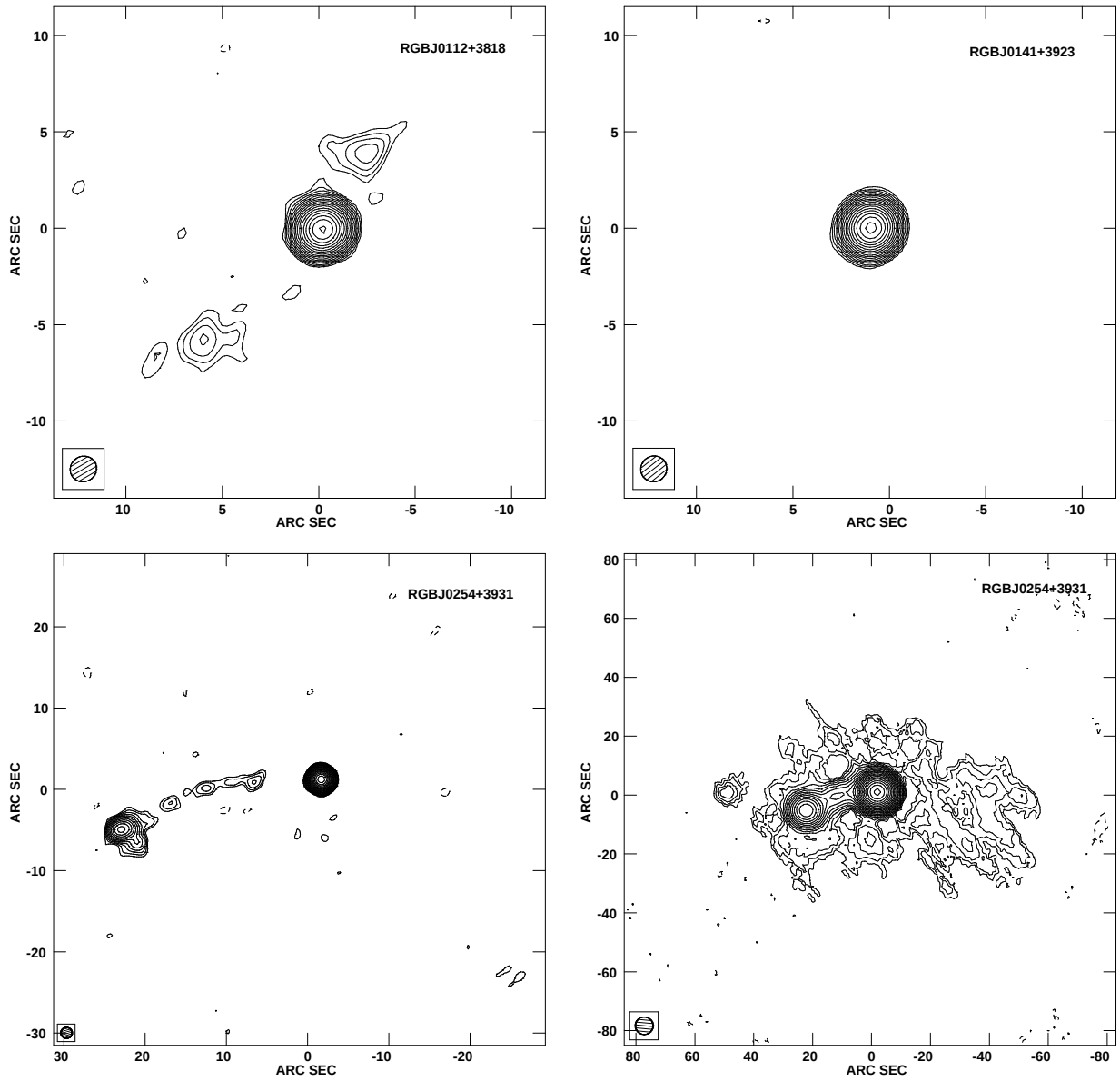

Fig. 1.— (a) RGB J0112+3818, VLA A. Image rms is 0.04 mJy/beam. Image peak is 32.5 mJy/beam. (b) RGB J0141+3923, VLA A. Image rms is 0.12 mJy/beam. Image peak is 104.5 mJy/beam. (c) RGB J0254+3931, VLA A. Image rms is 0.08 mJy/beam. Image peak is 160.2 mJy/beam. (d) RGB J0254+3931, VLA A+C. Image rms is 0.07 mJy/beam. Image peak is 167.5 mJy/beam. In all images contours start at 3 times the rms and positive values are spaced by factors of $\sqrt{2}$ up to the image peak.

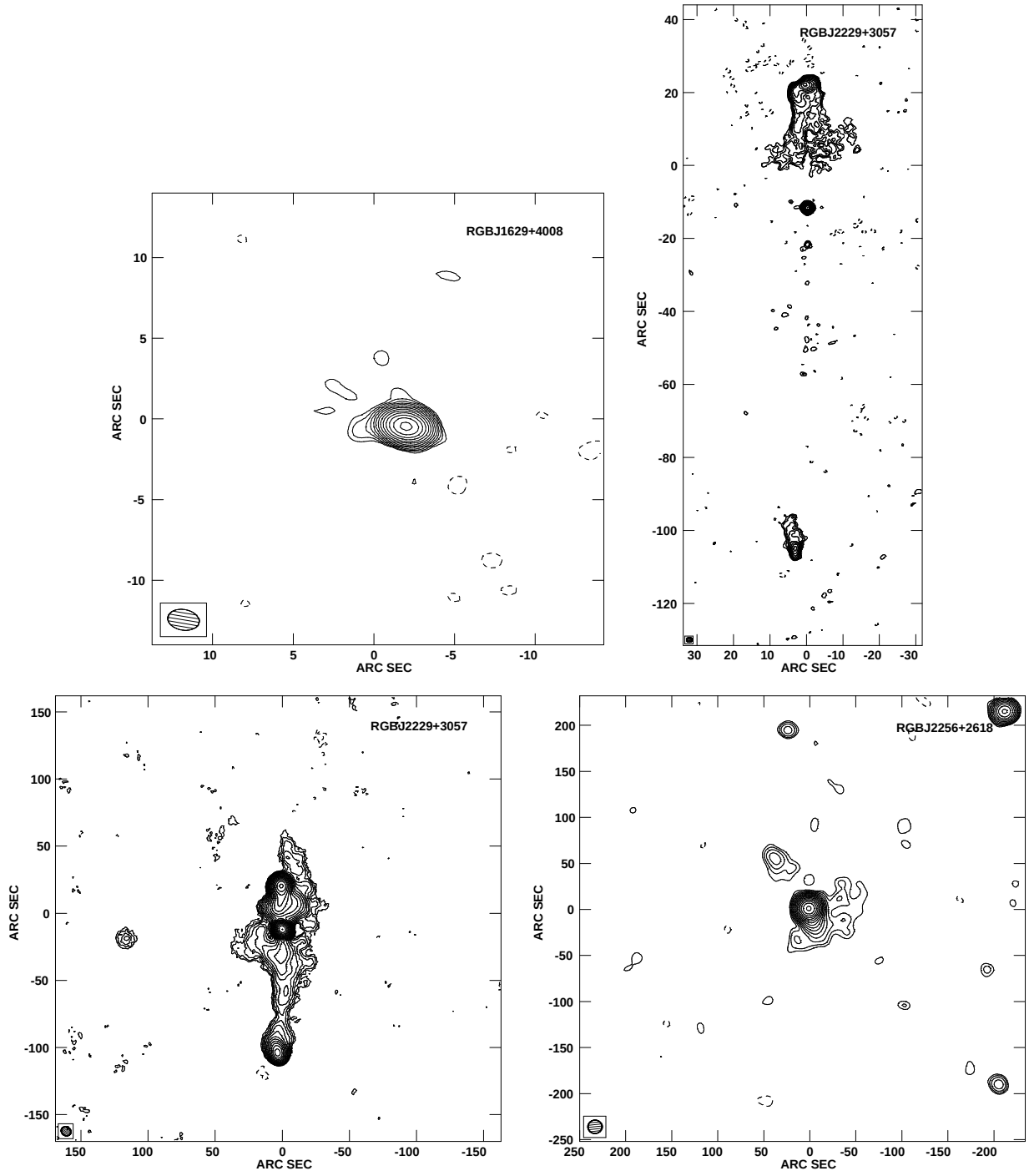

Fig. 1.— (e) RGB J1629+4008, VLA A. Image rms is 0.04 mJy/beam. Image peak is 8.6 mJy/beam. (f) RGB J2229+3057, VLA A. Image rms is 0.04 mJy/beam. Image peak is 44.2 mJy/beam. (g) RGB J2229+3057, VLA A+C. Image rms is 0.04 mJy/beam. Image peak is 44.2 mJy/beam. (h) RGB J2256+2618, VLA C. Image rms is 0.06 mJy/beam. Image peak is 24.7 mJy/beam. In all images contours start at 3 times the rms and positive values are spaced by factors of $\sqrt{2}$ up to the image peak.

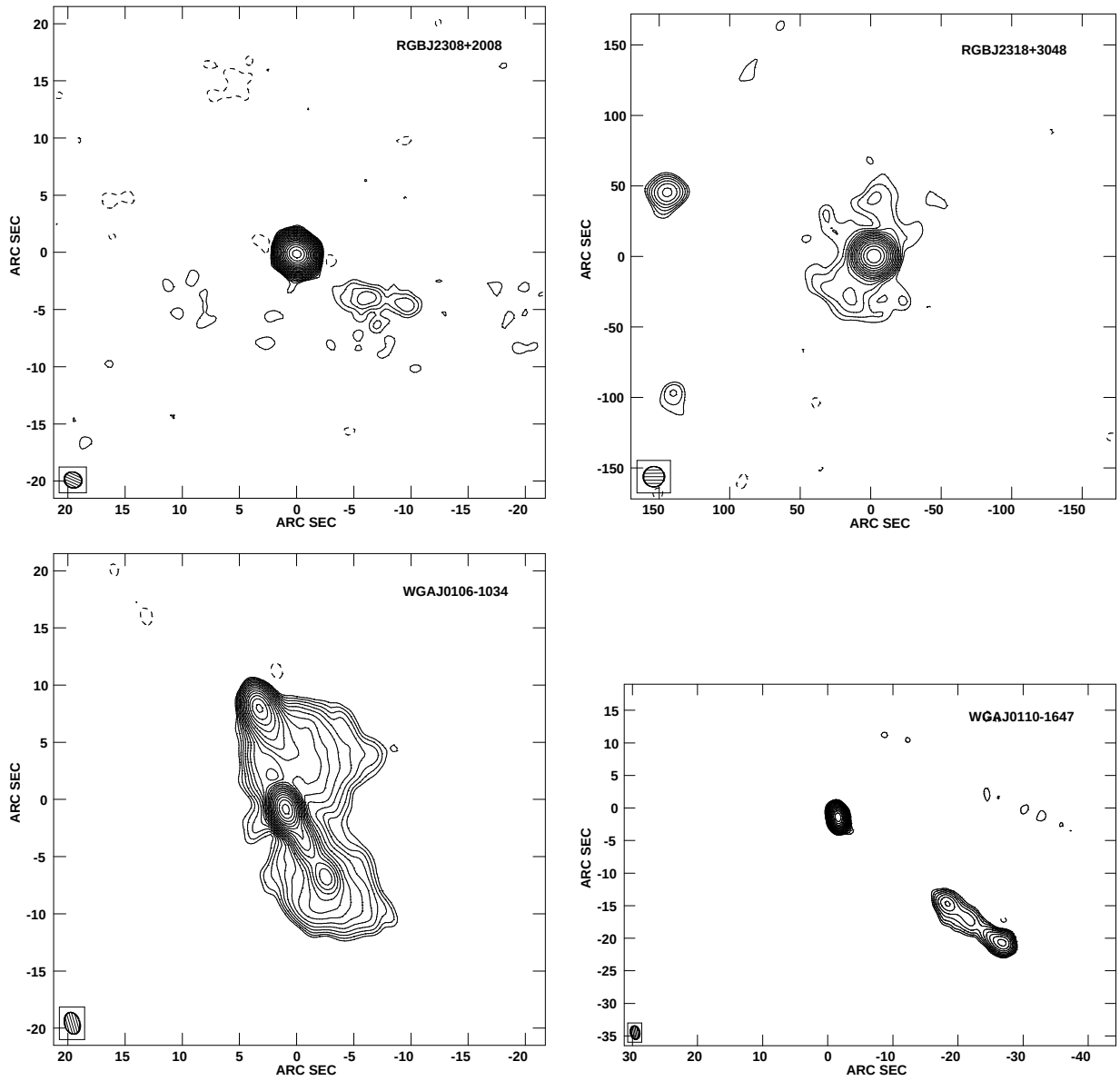

Fig. 1.— (i) RGB J2308+2008, VLA A. Image rms is 0.06 mJy/beam. Image peak is 218.0 mJy/beam. (j) RGB J2318+3048, VLA C. Image rms is 0.06 mJy/beam. Image peak is 22.2 mJy/beam. (k) WGA J0106−1034, VLA A. Image rms is 0.03 mJy/beam. Image peak is 105.5 mJy/beam. (l) WGA J0110−1647, VLA A. Image rms is 0.10 mJy/beam. Image peak is 72.0 mJy/beam. In all images contours start at 3 times the rms and positive values are spaced by factors of $\sqrt{2}$ up to the image peak.

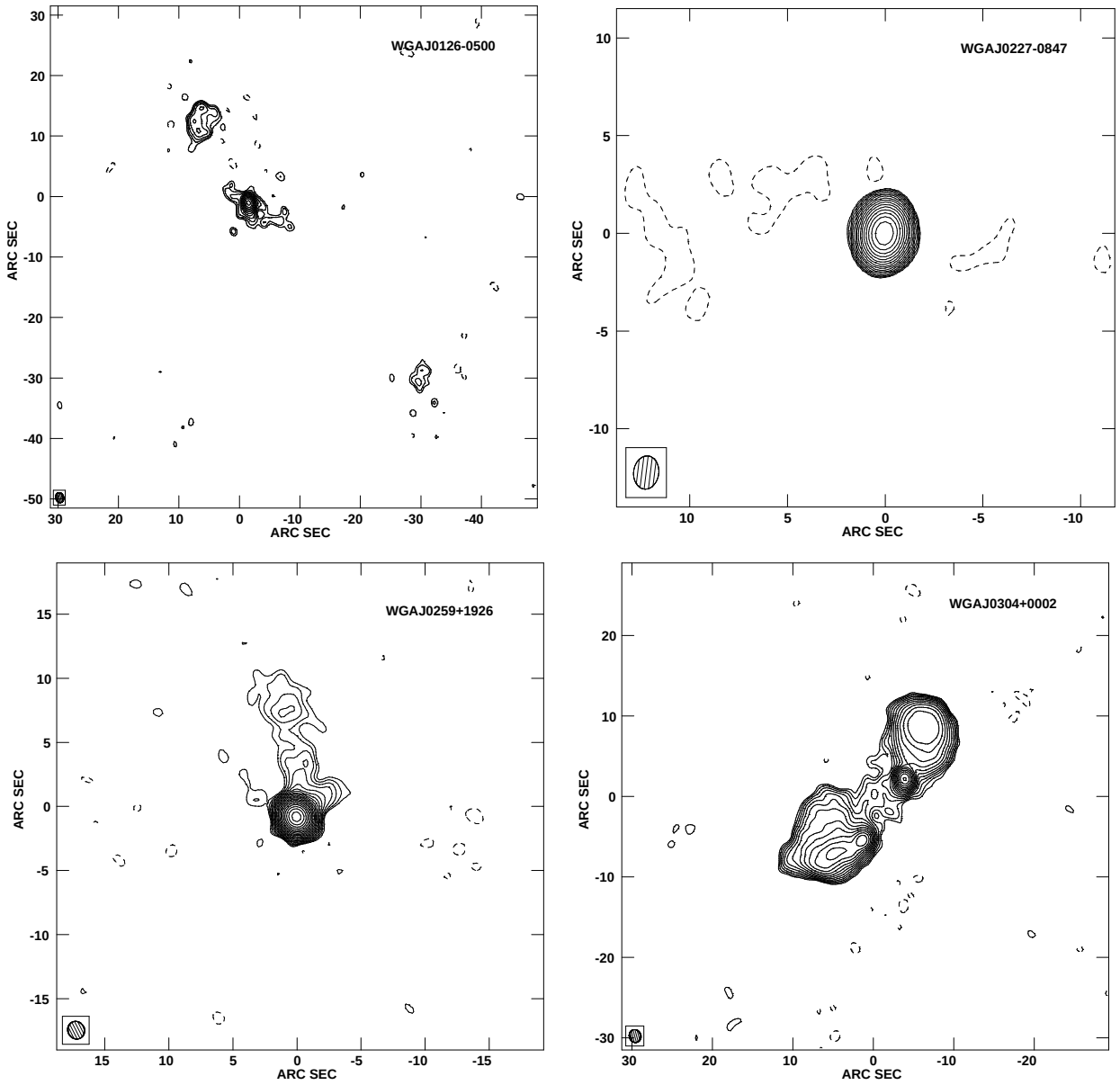

Fig. 1.— (m) WGA J0126−0500, VLA A. Image rms is 0.13 mJy/beam. Image peak is 14.6 mJy/beam. (n) WGA J0227−0847, VLA A. Image rms is 0.10 mJy/beam. Image peak is 76.7 mJy/beam. (o) WGA J0259+1926, VLA A. Image rms is 0.05 mJy/beam. Image peak is 133.1 mJy/beam. (p) WGA J0304+0002, VLA A. Image rms is 0.03 mJy/beam. Image peak is 8.4 mJy/beam. In all images contours start at 3 times the rms and positive values are spaced by factors of $\sqrt{2}$ up to the image peak.

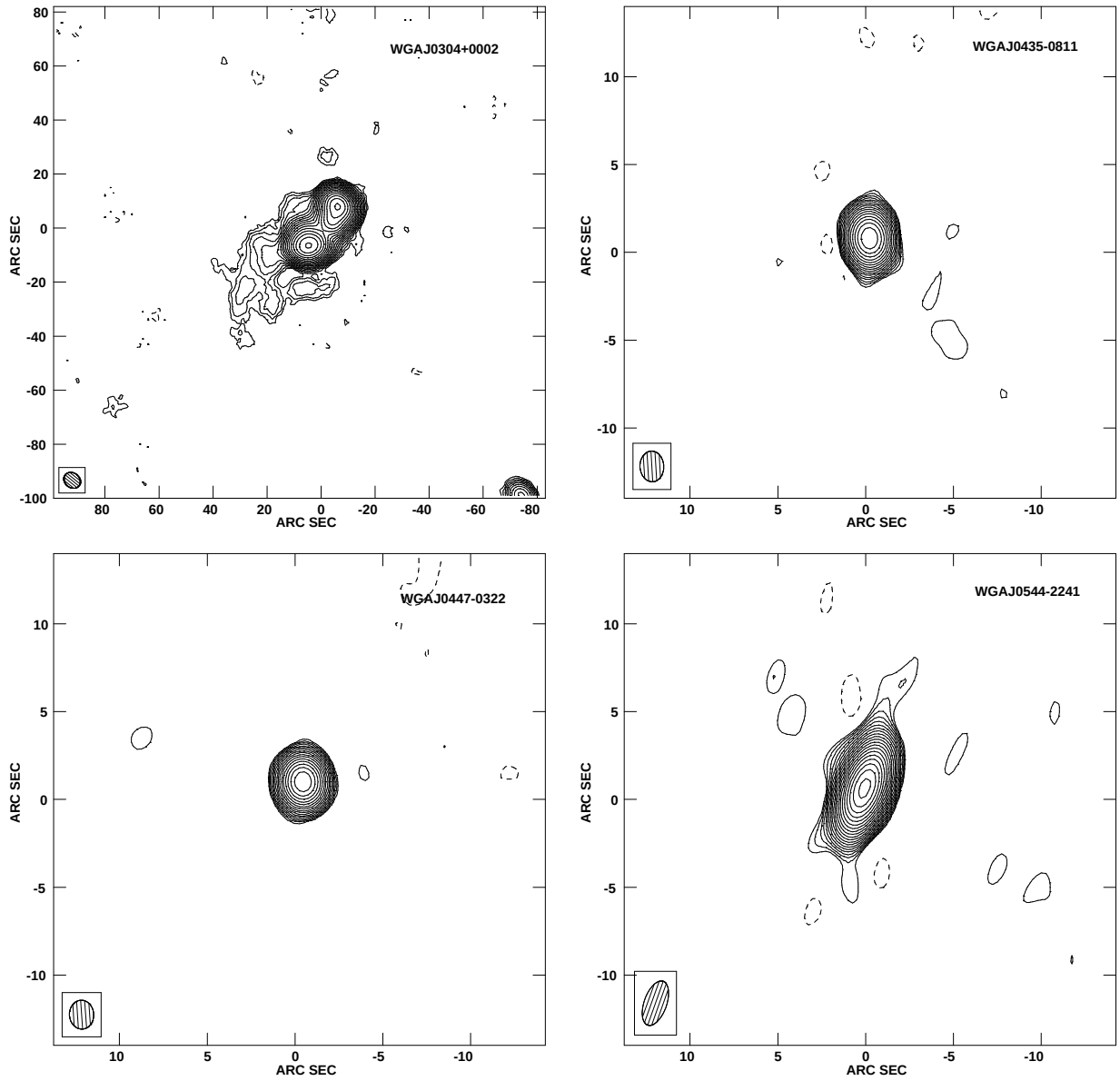

Fig. 1.— (q) WGA J0304+0002, VLA A+C. Image rms is 0.04 mJy/beam. Image peak is 29.1 mJy/beam. (r) WGA J0435−0811, VLA A. Image rms is 0.04 mJy/beam. Image peak is 30.3 mJy/beam. (s) WGA J0447−0322, VLA A. Image rms is 0.09 mJy/beam. Image peak is 68.0 mJy/beam. (t) WGA J0544−2241, VLA A. Image rms is 0.06 mJy/beam. Image peak is 149.6 mJy/beam. In all images contours start at 3 times the rms and positive values are spaced by factors of $\sqrt{2}$ up to the image peak.

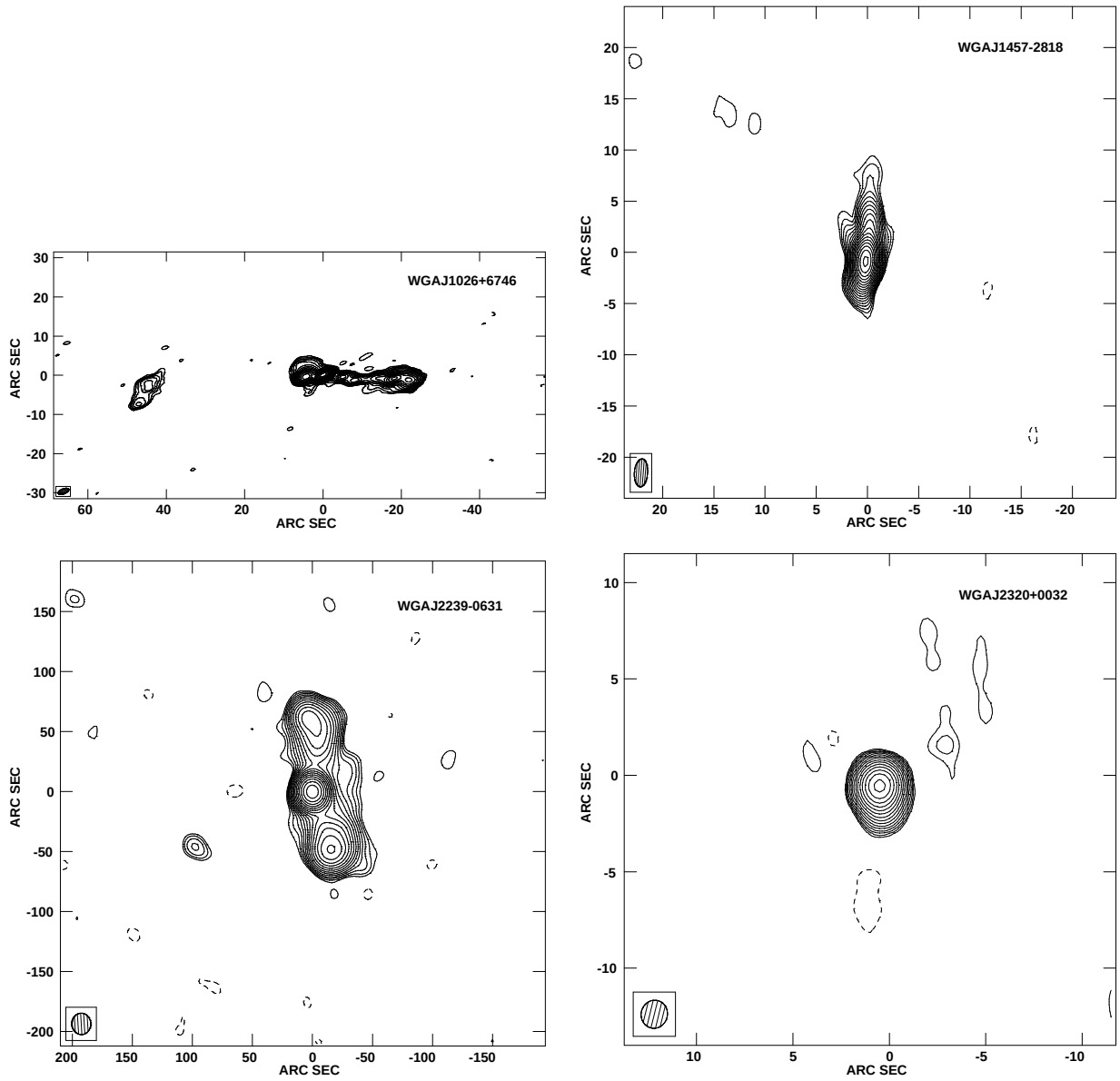

Fig. 1.— (u) WGA J1026+6746, VLA A. Image rms is 0.12 mJy/beam. Image peak is 84.7 mJy/beam. (v) WGA J1457−2818, VLA A. Image rms is 0.16 mJy/beam. Image peak is 190.4 mJy/beam. (w) WGA J2239−0631, VLA C. Image rms is 0.07 mJy/beam. Image peak is 52.6 mJy/beam. (x) WGA J2320+0032, VLA A. Image rms is 0.15 mJy/beam. Image peak is 65.6 mJy/beam. In all images contours start at 3 times the rms and positive values are spaced by factors of $\sqrt{2}$ up to the image peak.

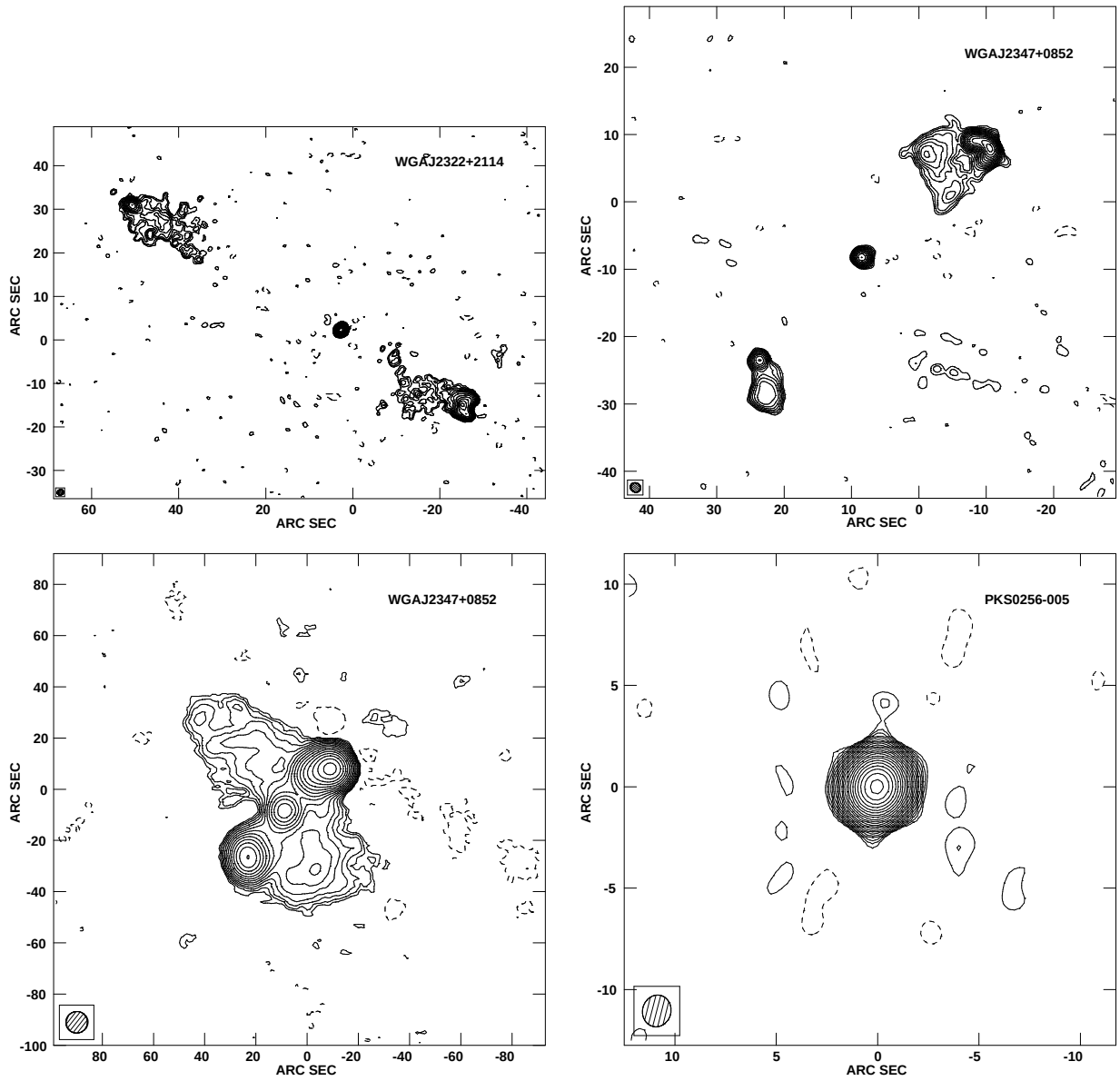

Fig. 1.— (y) WGA J2322+2114, VLA A. Image rms is 0.04 mJy/beam. Image peak is 40.4 mJy/beam. (z) WGA J2347+0852, VLA A. Image rms is 0.06 mJy/beam. Image peak is 19.4 mJy/beam. (aa) WGA J2347+0852, VLA A+C. Image rms is 0.08 mJy/beam. Image peak is 52.3 mJy/beam. (ab) PKS 0256−005, VLA A. Image rms is 0.05 mJy/beam. Image peak is 252.1 mJy/beam. In all images contours start at 3 times the rms and positive values are spaced by factors of $\sqrt{2}$ up to the image peak.

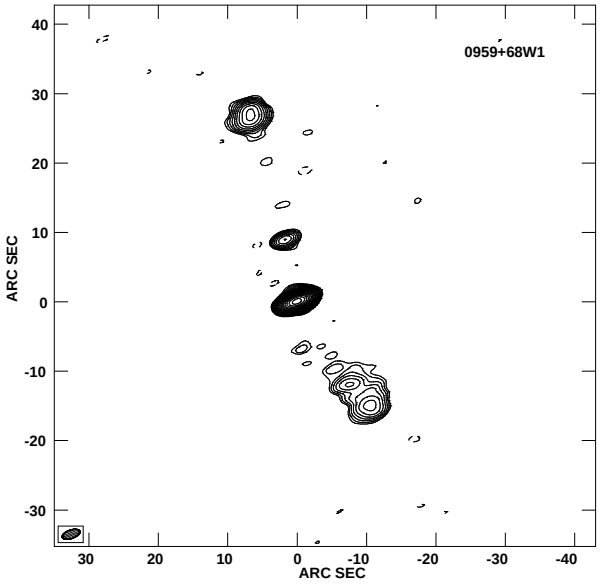

Fig. 1.— (ac) 0959+68W1, VLA A. Image rms is 0.06 mJy/beam. Image peak is 80.1 mJy/beam. Contours start at 3 times the rms and positive values are spaced by factors of $\sqrt{2}$ up to the image peak.

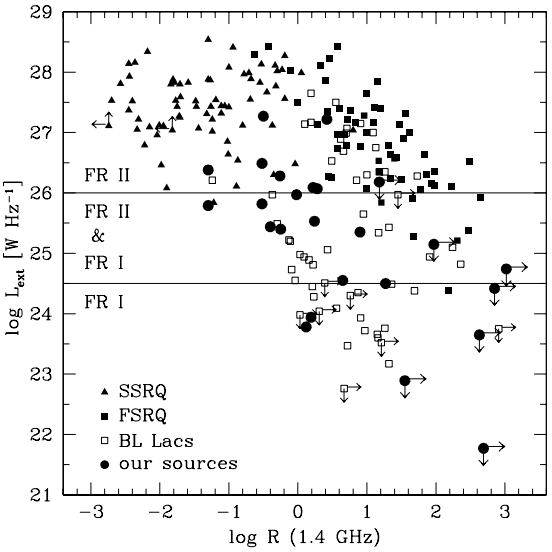

Fig. 2.— The extended radio power versus the radio core dominance parameter R at 1.4 GHz, where $R = L_{\rm core}/L_{\rm ext}$, with $L_{\rm core}$ and $L_{\rm ext}$ the radio core and extended luminosities, respectively. Filled triangles and squares indicate steep-spectrum (SSRQ) and flat-spectrum radio quasars (FSRQ), respectively, open squares indicate BL Lacs. See text for details on the selected samples. Large filled circles represent the sources in our sample. Arrows indicate limits. The horizontal solid lines mark the regions of extended radio powers typical of FR I and FR II radio galaxies.

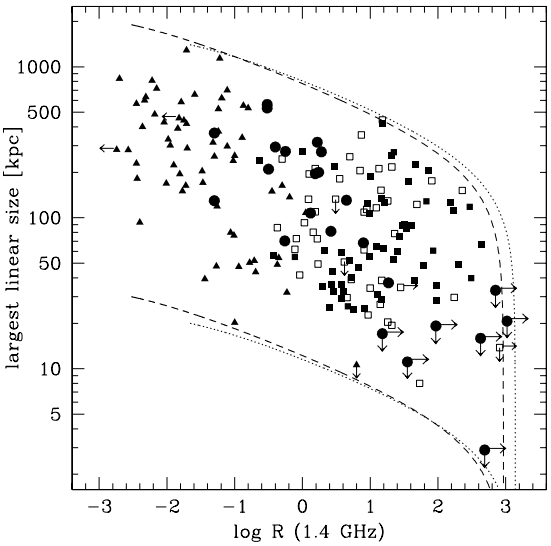

Fig. 3.— The largest linear size (LLS) versus the radio core dominance parameter R at 1.4 GHz. Symbols are as in Fig. 2. The dotted and dashed lines represent LLS $-$ R relations predicted by the relativistic beaming model for FR I and FR II radio galaxies, respectively, assuming different intrinsic largest linear sizes. See text for details.

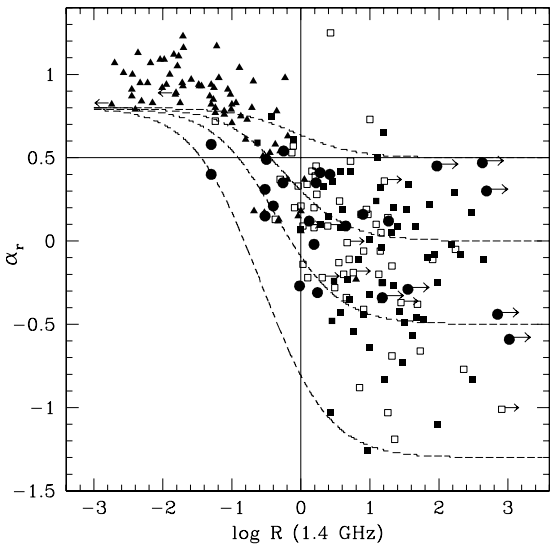

Fig. 4.— The radio spectral index versus the radio core dominance parameter R at 1.4 GHz. Symbols are as in Fig. 2. The vertical solid line separates lobe- (left of the line) from core-dominated sources (right of the line). The horizontal solid line indicates the locus of constant $\alpha_r = 0.5$. Radio-loud AGN below this line are currently defined as blazars. The dashed lines represent $\alpha_r - R$ relations for different values of the core radio spectral index of 0.5, 0, −0.5, and −1.3 (from top to bottom).

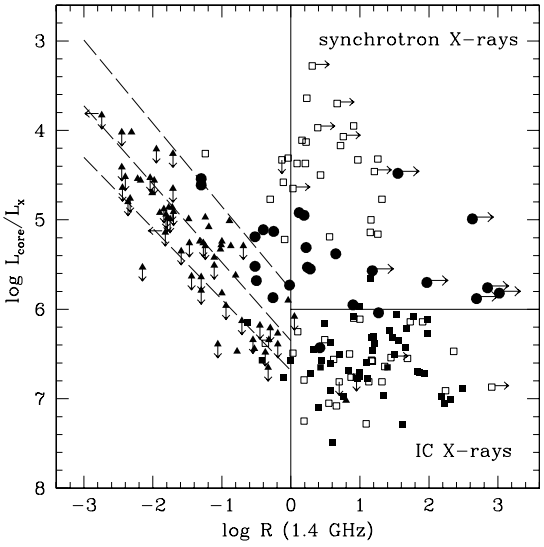

Fig. 5.— The ratio of radio core emission at 1.4 GHz to total X-ray luminosity at 1 keV versus the radio core dominance parameter R at 1.4 GHz. Symbols are as in Fig. 2. The vertical solid line separates lobe- (left of the line) from core-dominated sources (right of the line). The horizontal solid line separates sources with jet X-ray emission dominated by the synchrotron (above the line) and inverse Compton process (below the line). The dashed lines represent significant correlations for our lobe-dominated sources, SSRQ with detected X-rays, and all SSRQ (from top to bottom).